THE ASTROPHYSICAL JOURNAL, 472:183–190, 1996 November 20

LUMINOSITY FUNCTION OF THE PERIGALACTOCENTRIC REGION

VIJAY K. NARAYANAN, ANDREW GOULD,[1] AND D. L. DEPOY
Department of Astronomy, Ohio State University, Columbus, OH 43210;
vijay@payne.mps.ohio-state.edu, gould@payne.mps.ohio-state.edu, depoy@payne.mps.ohio-state.edu
Received 1996 April 2; accepted 1996 June 6

ABSTRACT

We present H and K photometry of $\sim$42,000 stars in an area of $\sim$250 arcmin^2 centered on the Galactic center. We use the photometry to construct a dereddened K-band luminosity function (LF) for this region, excluding the excessively crowded inner 2′ of the Galaxy. This LF is intermediate between the LF of Baade's window and the LF of inner 2′ of the Galactic center. We speculate that the bright stars in this region have an age that is intermediate between the starburst population in the Galactic center and the old bulge population. We present the coordinates and magnitude for 16 stars with $K_0 \leq 5$ for spectroscopic follow-up.

Subject headings: Galaxy: center — infrared: stars — stars: fundamental parameters — stars: luminosity function, mass function

1. INTRODUCTION

The 2.2 μm luminosity functions (LFs) of Baade's window (BW) and the inner 2′ of the Galactic center (GC) are markedly different at the bright end. The GC LF has a substantially higher fraction of stars brighter than $K_0 = 5.5$, but it is nearly identical to the BW LF at the faint end for $K_0 >$ 7.0. This suggests that the GC contains a population of younger stars in addition to an older population of red giants similar to the one in BW (Haller 1992; Blum, Sellgren, & DePoy 1996). Here we present H and K photometry of $\sim$42,000 stars in an area of $\sim 16' \times 16'$ centered on the GC. In our analysis, we exclude the inner 2′ and refer to the remaining area as the perigalactocentric region (PGC). We construct the K-band LF of the PGC by dereddening each star individually using its observed $H-K$ colors. We find that the PGC does not contain any superbright stars of the type found in the GC. For $K_0 < 6.0$, the GC LF has a significant excess over the PGC LF. In comparing the PGC with BW, we find that for BW the contamination by the foreground distribution of M giants is significant for $K_0 < 7.0$, while for the PGC it is negligible. Even if the contamination in BW is neglected, there is still a clear excess of stars in the PGC over BW in the range $4.0 < K_0 < 7.0$. We conclude that the luminosity function of the PGC is intermediate between that of the GC and Baade's window.

2. OBSERVATIONS AND MOSAIC CONSTRUCTION

We constructed mosaic images of the GC and PGC in H and K bands by stitching together $8 \times 19 = 152$ overlapping images. The grid of images was taken on UT 1995 June 10 and 11 using the Ohio State Infrared Imaging Spectrograph (OSIRIS; DePoy et al. 1993a) at the 1.8 m Perkins Telescope, located on Anderson Mesa near Flagstaff, Arizona. OSIRIS uses a 256 × 256 NICMOS III array. All the images were taken under photometric conditions. The plate scale is $\sim$0″.63 per pixel ($\sim$155″ field of view). Images in the same row are offset by $\sim$50″, while those in the same column are offset by $\sim$120″. The images were exposed successively without any intervening sky exposures. The seeing was between 1″.4 and 2″.4 in H and between 2″.1 and 2″.8 in K. We constructed the H and K mosaics independently. A standard star, P565-C, was observed both before and after the observations in the H band and after the observations in the K band. Each exposure was $\sim$1.1 s long. We co-added 10 individual exposures to form each individual image. The sky image formed from the median of the standard star images was subtracted from each of the raw images. Finally, we divided the images by a flat field formed from the median of the images of a white screen mounted to the telescope. We aligned the images geometrically and photometrically before making the final mosaic.

The global solution for the geometric and photometric offsets between the images was used to construct the mosaic in the H and K bands. In combining the pixels, we averaged all the contributing pixel values, after rejecting the pixel values that were more than 5 σ away from the mean of the remaining pixel values, where σ is computed assuming photon counting statistics. In the case of bright stars, we accepted all the contributing pixel values to ensure that the flux of the star is conserved. Some of the individual H-band images contain interference fringes from variable OH emission with typical amplitude of $\sim$6 ADU and width of $\sim$15 pixels. Fringes of this type are often removed from H-band images by chopping to the sky. As noted above, we did not chop. However, the typical amplitude of the fringes in the mosaic image is only $\sim$2 ADU (since typically each pixel in the final mosaic is an average of pixels in three individual images), corresponding to $H \sim 19$ mag arcsec^{-2}, and hence it is too small to affect the results.

The H and K mosaics are shown in Figures 1 and 2, respectively. The K mosaic is offset by $\sim$40″ to the west relative to the H mosaic. Excluding the rim of the mosaic in which there is information from only one image, about 60% of the area of each mosaic is constructed from three overlapping images, and the other 40% is constructed from six images. The typical sky level is $\sim$14 mag arcsec^{-2} in the H mosaic and $\sim$12 mag arcsec^2 in the K mosaic. One ADU corresponds to $\sim$21 mag arcsec^{-2} in H and $\sim$20.4 mag arcsec^{-2} in K. There is a difference of $\sim$2–3 ADU across the seams in the final mosaic, of order 1% of the sky.

3. PHOTOMETRY

We initially identified $\sim$28,000 candidate stars in the H mosaic using the DAOFIND routine of DAOPHOT

[1] Alfred P. Sloan Foundation Fellow.

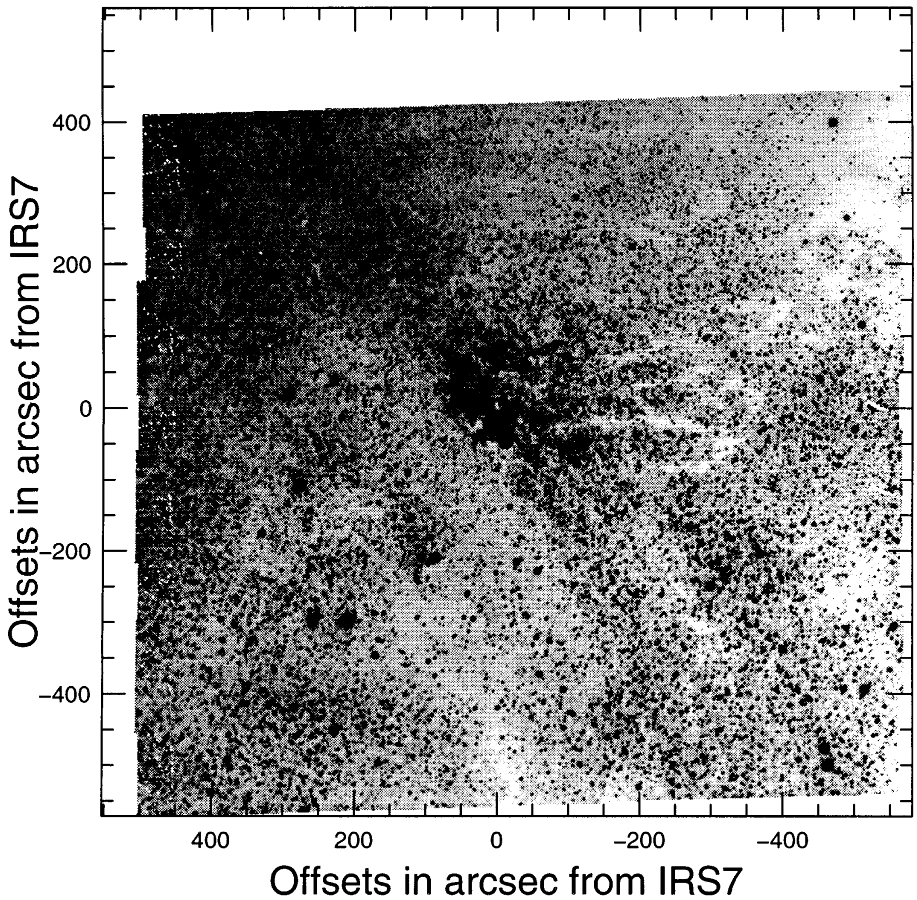

FIG. 1.—*H*-band mosaic image. North is up and east is left. The coordinates are offsets in arcseconds from IRS 7.

(Stetson 1987). The extinction pattern in the images has many patchy and filamentary structures on small scales. For stars in these highly obscured patches, the local sky determined from an annular region around the star by DAOPHOT was often greater than the peak flux of the star itself. These stars were either not identified or photometered incorrectly by DAOPHOT. Therefore, we identified the stars not found by DAOFIND manually by displaying the *H* mosaic in various stretches of brightness levels. We used the *K* mosaic to help identify the faint stars in some heavily obscured regions. However, the sample of stars is essentially *H*-band–selected because of better seeing in *H*. Finally, we identified a total of $\sim$65,000 candidate stars.

The photometry was carried out by extracting small, overlapping sections of 100 × 100 pixels from the *H*- and *K*-band mosaics. The overlap between the neighboring sections is 5 pixels in both the horizontal and vertical directions. There are 342 such sections in each band. Each of these sections was photometered independently. In each section, only the stars that lie within the inner 95 × 95 pixels were accepted in the final photometry list. We measured the *H* and *K* magnitudes of the stars by fitting the stellar profiles to an appropriate point-spread function (PSF) and the local sky. The instrumental magnitudes determined from this PSF fitting were converted to apparent magnitudes using aperture photometry of PSF stars compared to the standard stars.

The observations were carried out at $\sim$2 air masses, while the standard star was observed at $\sim$1 air mass. Therefore, we applied an air-mass correction of 0.1 mag in both *H* and *K* bands. There is a residual uncertainty of $\sim$0.03 mag in the photometric zero points because of the uncertainty in the appropriate value of this correction.

3.1. *H Band*

The seeing in *H* band changed significantly during the approximately 2 hr period of observations. Therefore, we identified 98 stars that were well isolated and bright enough that they were not contaminated by the light from neighboring stars. These PSF stars are spread approximately uniformly throughout the *H* image. The stars in each of the 342 small sections were photometered by using a PSF that was most similar to the PSF for that section. Except in a few cases in which the seeing changed abruptly, the PSF nearest to a section was adequate for this purpose.

We fitted all the stars in a section simultaneously. Starting from the approximate coordinate locations, we first fitted each star to four parameters: three parameters that model the sky (including a constant offset and linear terms in the horizontal and vertical directions) and one parameter for the PSF normalization. With these parameters, we then found the best values for the coordinate locations of the star by shifting the stellar profile by fractional pixel amounts and minimizing the χ^2 difference between the fit and the image. This best fit for the star is then subtracted from the image. All the stars are fitted and subtracted from the original image in this manner to create a residual image.

The brightest star was then added to this residual image. It was fitted again for all the six parameters that define the PSF normalization, the local sky, and the best coordinate

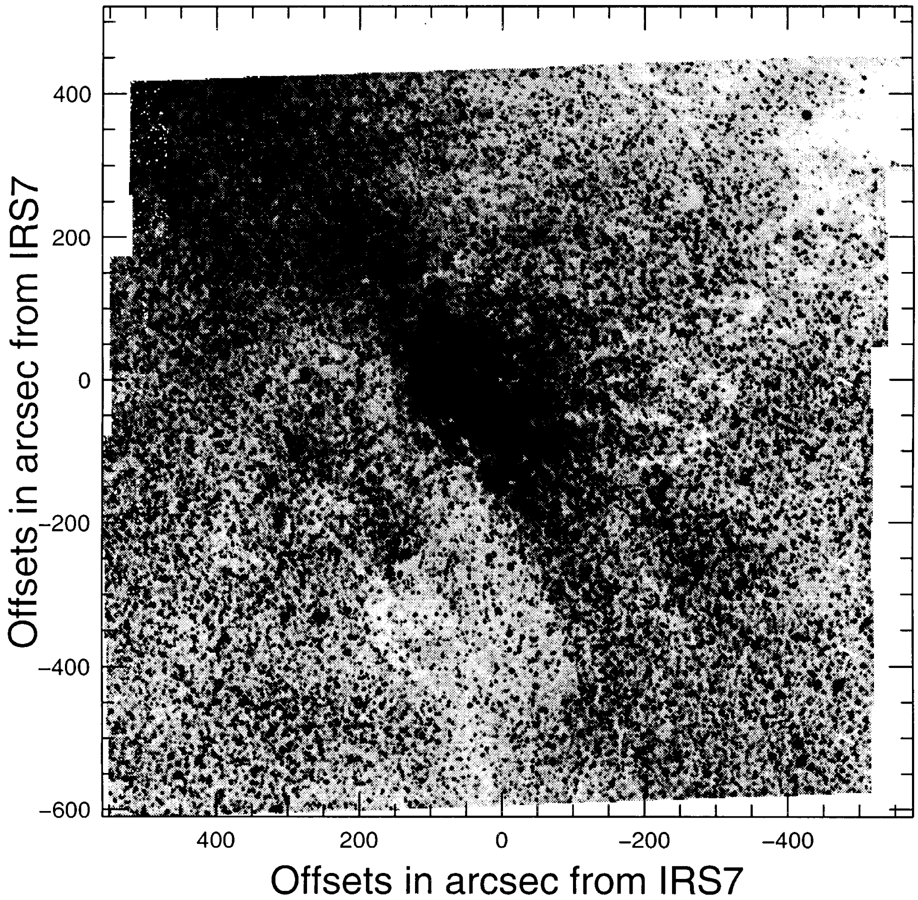

FIG. 2.—K-band mosaic imge. North is up and east is left. The coordinates are offsets in arcseconds from IRS 7.

locations in the same manner as described above, and this best fit was again subtracted from the residual image. This procedure was repeated for all the other stars in order of their decreasing brightness as determined from the first pass. Therefore, before we fitted for any star, all its brighter neighbors would have already been measured and their fluxes subtracted, thereby reducing the contamination from neighbors.

3.2. *K Band*

The K mosaic is distorted by $\sim 0.1\%$ with respect to the H mosaic. We determined a linear transformation between H and K mosaics, using the locations of 142 bright stars. The distortion was largely removed by this transformation, as was verified by the residuals of the fit. The seeing in K band is worse than in the H band. There are only a few isolated stars that are not contaminated by neighboring stars. However, the seeing remained approximately constant throughout the K-band observations. Therefore, all the stars in the K band were fitted to five different PSFs in a manner similar to the H photometry. In this fitting procedure, however, we assumed that the transformed locations of the stars are accurate enough. For each star photometered in H, we assumed that the K mosaic also contained the star at the corresponding transformed location. Therefore, each star was fitted for four parameters only. We take the average of these five measurements (after rejecting 3 σ outliers) to be the K magnitude. We estimate the error in the K photometry as the standard deviation of the five measurements averaged over the stars in a given magnitude bin (Fig. 3).

3.3. *Errors in the Photometry*

H and K magnitudes are measured for $\sim 42{,}300$ stars in the entire field. The other candidates are either misidentifications or are too faint in one of the bands to be measured by this method. The errors in H band are assumed to be the same as the errors in K band.

The photometric errors in both bands depend on the crowding of stars. Very close to the GC, the photometry is

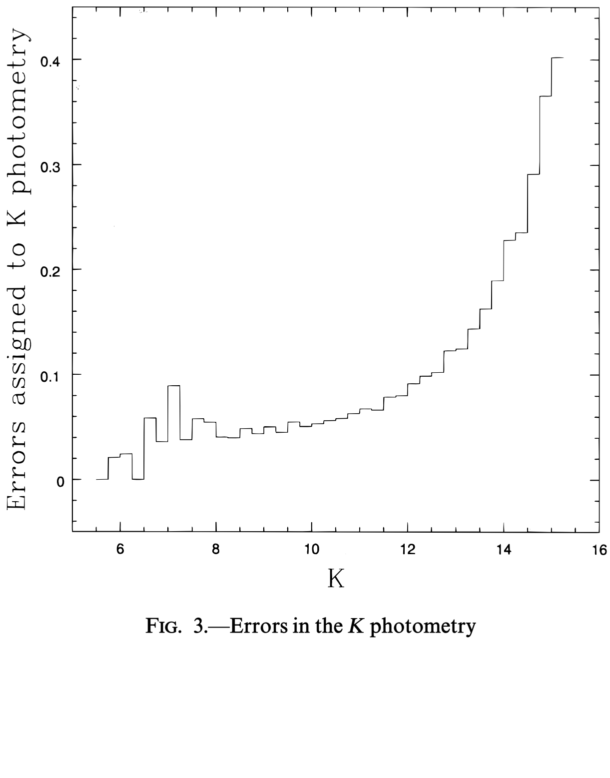

FIG. 3.—Errors in the K photometry

limited by our ability to identify separate stars. Excessive crowding of stars, together with the relatively poor seeing, made it difficult to separate the objects into individual stars. The results reported here are based on photometry of regions more than 2′ away from the GC.

4. DEREDDENED MAGNITUDES

The observed $H-K$ color of a PGC star is the sum of the intrinsic color, $(H-K)_0$, and the selective extinction coefficient, $E(H-K)$. Therefore, we deredden the PGC stars individually by using the observed $H-K$ colors and an appropriate color-magnitude relation. We use the near-infrared extinction law determined by Mathis (1990) to compute the total extinction coefficients A_K and A_H. Specifically, we assume $A_H/A_K = 1.66$ and $A_K = 1.5E(H-K)$.

We assume that the intrinsic color-magnitude relation for stars in PGC (corrected for extinction) is the same as that of stars in BW. We fitted a color-magnitude relation for stars in BW, using the photometry provided to us by J. Frogel (1995, private communication), to obtain the following analytic relation:

$$K_0 = -9(H-K)_0 + 10.7 \quad (K_0 < 8.5),$$
$$K_0 = -50(H-K)_0 + 18.0 \quad (K_0 > 8.5). \qquad (4.1)$$

All stars with $E(H-K) < 0.6$ are assumed to be foreground stars. There are 10 stars that are saturated either in the H or K mosaic, or in both. Therefore, we divided the H mosaic by the K mosaic and determined the colors of these stars by estimating the color at the wings, where the pixel counts are not saturated. We estimated the colors at the wings by comparing them with nearby stars that were not saturated. Only one of these 10 stars is sufficiently reddened to be a PGC star.

5. LUMINOSITY FUNCTION OF THE PGC

The PGC suffers from very patchy extinction. As a result, the completeness level of our photometry can change drastically throughout the imaged region. Therefore, we identified six regions around the GC that have moderate ($A_K \sim 2.7$) and roughly homogeneous extinction (collectively called Reg1). While Reg1 does contain a few patches of high extinction, these patches are very small and do not affect our results. Reg1 encloses about 5% of the total area of the PGC. The six regions comprising Reg1 are chosen at more than 2′ away from the GC, so the photometry does not suffer from the severe crowding of the GC. All the Reg1 stars with $K_0 \leq 8.0$ were examined individually, and the bad photometry cases were rejected. The color-magnitude diagram of patch 1 of Reg1 is shown in Figure 4. In order to be able to compare the Reg1 LF with that of BW and GC, we normalize the star counts in a given region by the integrated K-band flux (corrected for extinction) falling in that region. We determine the dereddened flux as follows: In each of the six regions comprising Reg1, we compute the mean $\bar{E}(H-K)$ of stars from the mean offset in $H-K$ relative to the giants in BW. Then we find the total flux within the region and multiply this by $10^{0.4\bar{A}_K}$, where $\bar{A}_K = 1.5\bar{E}(H-K)$. We estimate the true sky by measuring the counts in heavily extincted regions. This gives an upper limit to the true sky, as there is some K light from the bulge even in heavily extincted regions. This sky is then used to estimate the counts due to bulge light in lightly extincted regions with a small fractional error due to the uncertain sky. By comparing the extinctions in these two regions (measured

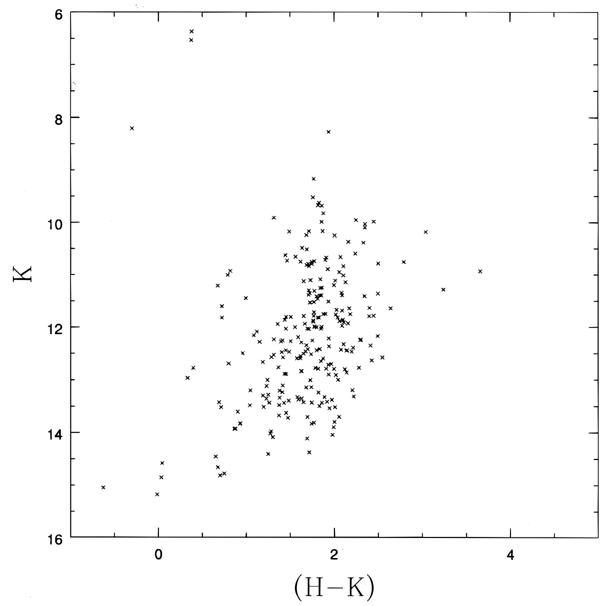

FIG. 4.—Color-magnitude diagram of patch 1 of Reg1

from the reddening of bright stars), we can estimate accurately the small amount of K light from the bulge in the heavily extincted region. We estimate the errors in this procedure to be ~ 3 ADU pixel^{-1}. This leads to an uncertainty of $\sim 2\%$ in the total flux, negligible compared to other errors.

To verify the accuracy of this LF of the PGC, we also identified another 22 regions of moderate reddening (Reg2), covering another 20% of the total area of the PGC. All stars with $K_0 \leq 6.5$ in these regions were examined individually, and the LF was constructed in a similar manner. The LFs determined for Reg1 and Reg2 are shown in Table 1 and are plotted in Figure 5. The two LFs are identical within Poisson errors.

The H and K mosaics give the visual impression of a disklike feature approximately aligned with the Galactic plane (Figs. 1 and 2). In order to check if the stellar popu-

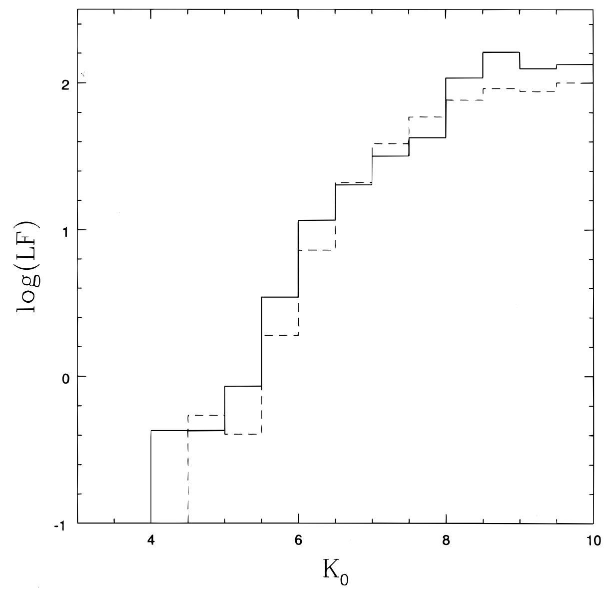

FIG. 5.—Comparison of the LFs from two different regions of PGC: Reg1 (*solid line*) and Reg2 (*dashed line*). The two LFs are identical within Poisson errors.

TABLE 1

LFs and the Number of Stars Observed in Each Half-Magnitude Bin[a]

	PGC							
	Reg1		Reg2		GC		BW[b]	
K_0	LF	N	LF	N	LF	N	LF	N
1.75......	0	0	0	0	0.46	1	0	0
2.25......	0	0	0	0	0.00	0	0	0
2.75......	0	0	0	0	0.91	2	0	0
3.25......	0	0	0	0	0.46	1	0	0
3.75......	0	0	0	0	1.83	4	0	0
4.25......	0.43	1	0	0	0.92	2	0	0
4.75......	0.43	1	0.54	4	3.66	8	0	0
5.25......	0.86	2	0.41	3	5.03	11	0	0
5.75......	3.47	8	1.90	14	10.05	22	2.56	1
6.25......	11.60	26	7.24[c]	53	10.51	23	0.92	1
6.75......	20.25	46	20.96	179	34.29	75	7.01	4
7.25......	31.80	71	38.63	328	53.03	116	51.22	14
7.75......	42.36[c]	94	58.50	495	64.10	139	52.12	15
8.25......	107.83	210	76.48	645	84.74	187	49.92	10
8.75......	161.09	274	91.67	772	97.83	214	104.77	14
9.25......	124.74	209	87.21	800	128.92	282	198.20	340
9.75......	133.63	215	99.84	916	146.29	320	287.50	505
10.25......	127.93	212	84.58	776	122.06	267	431.24	663
10.75......	156.64	196	80.88	742	65.37	143	574.98	925
11.25......	125.91	152	72.48	665	30.63	67	718.74	1309
11.75......	90.31	112	59.85	549	13.25	29	1006.23	1786

[a] For the two sets of regions of PGC, the inner 2′ of GC and BW.

[b] For $5 \leq K_0 \leq 9$, the photometry is from FW87. For $9 \leq K_0 \leq 12$, the photometry is from DePoy et al. 1993b.

[c] Stars in this bin and brighter were examined individually. For fainter magnitudes, we applied statistical corrections. For $9 \leq K_0 \leq 12$, the photometry is from DePoy et al. 1993b.

lation of this feature is different from the surrounding regions, we selected all the Reg1 regions from within the apparent disk and all the Reg2 regions from outside it. The centroids and areas of the six patches comprising Reg1 and the 22 patches comprising Reg2 are in Tables 2 and 3, respectively. The locations and geometries of these patches are shown in Figure 6. Although a few patches lie close to each other, they are reddened by different amounts. The LFs of these two regions are the same, indicating that the stellar populations at least of these two regions are indistinguishable.

6. COMPLETENESS LIMIT OF THE LF

The LF is based on stars selected in the H mosaic. Stars were identified first by using the DAOPHOT star finding routine DAOFIND and then by scanning the images manually to find the stars missed by DAOFIND. Based on the tests described below, we conclude that the LF is complete up to $K_0 = 8$.

We added 10 artificial stars per half-magnitude bin in H at random locations in each patch. We ran DAOFIND on the resulting images to determine the fraction of stars detected. For each undetected star, we judged whether we would have found the star in the manual search. Figure 7 shows the completeness of the DAOFIND and combined (DAOFIND plus manual) searches. The combined search is complete for $H < 12.5$ and $\sim 80\%$ complete at $H = 14$.

The DAOFIND completeness limit is objective, but the DAOFIND-plus-manual search limit depends in part on subjective judgment. To test whether this procedure repro-

TABLE 2

Reg1 Patches

Patch Identification	$\Delta\alpha$ (arcsec)	$\Delta\delta$ (arcsec)	Area (arcmin^2)
1.............	397.5	−422.5	1.98
2.............	249.9	−277.1	1.85
3.............	134.8	−221.6	2.51
4.............	140.6	−89.8	2.54
5.............	−139.0	205.3	2.25
6.............	−248.3	324.9	1.71

TABLE 3

Reg2 Patches

Patch Identification	$\Delta\alpha$ (arcsec)	$\Delta\delta$ (arcsec)	Area (arcmin^2)
1	129.1	−437.6	1.83
2	−116.6	−407.9	2.40
3	−261.6	−409.6	2.30
4	−125.5	−126.5	1.95
5	−198.1	−248.7	1.80
6	−333.9	−244.3	2.29
7	−224.5	−29.9	1.84
8	−381.1	−122.8	2.37
9	−357.5	95.6	2.71
10	−374.9	273.2	4.93
11	−435.2	123.9	2.69
12	460.7	−314.5	2.38
13	351.5	−183.6	2.49
14	424.6	−2.9	3.26
15	458.0	−146.5	1.98
16	220.0	57.3	1.10
17	306.3	225.3	2.64
18	470.7	128.0	2.05
19	340.3	293.9	2.61
20	184.2	302.4	2.73
21	−43.6	378.2	2.69
22	474.3	228.1	2.21

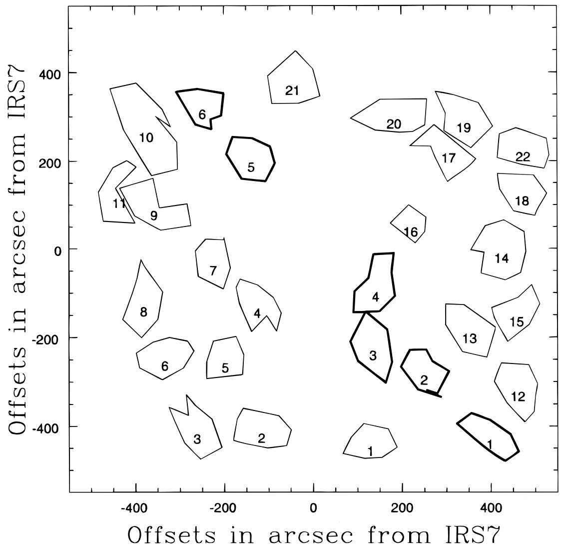

FIG. 6.—The six regions comprising Reg1 (*thick lines*) and the 22 regions comprising Reg2 (*thin lines*). North is up and east is left. Reg1 patches lie in the disklike feature in the K mosaic, while the Reg2 regions are outside it.

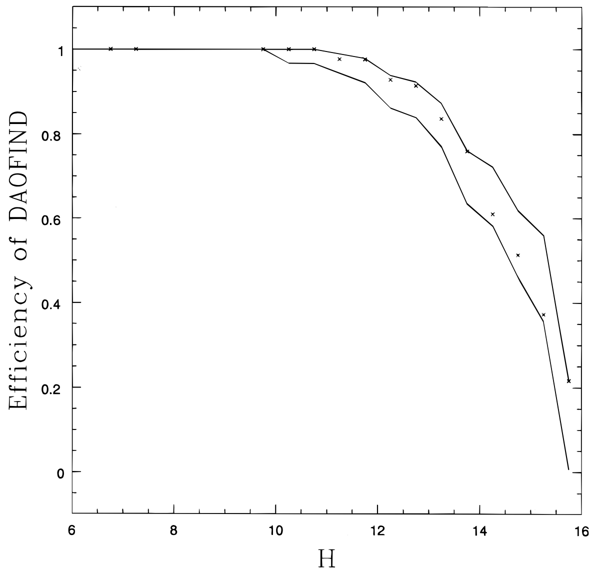

FIG. 8.—The two solid curves enclose the 1 σ bound of the DAOPHOT detection fraction determined from the artificial star tests. The points are the fraction for the sample star list.

duces the actual manual detection rate, we compared the fraction of stars that were undetected by DAOFIND but were found manually in the real data with the same fraction in the artificial star sample. The results of this test are shown in Figure 8. The sample star list fractions lie within 1 σ of the artificial star list fractions for all H. This consistency check confirms the accuracy of the combined (DAOFIND plus manual) detection efficiency.

To construct the LF, we weighed each detected star by the inverse of the completeness fraction corresponding to its H magnitude. The patches typically have $A_H \sim 4.5$. Therefore, the LF is fully complete for $K_0 < 8$. Due to the weighing procedure, we also expect the LF to be statistically complete for $8 < K_0 < 9$.

Some of the stars in the sample star list are bad identifications. For $K_0 < 8$, we found these by checking each star individually. For $K_0 > 8$, we applied the following statistical corrections: We selected 100 stars randomly in each of the magnitude ranges $8 < K_0 < 9$, $9 < K_0 < 10$, and $10 < K_0 < 11$. These stars were examined individually, and bad identifications were rejected. In these three magnitude ranges, we found 15%, 22%, and 22% of the total sample of stars to be bad identifications. For $K_0 > 11$, we assumed the bad identifications to be 22%. Therefore, we multiplied the LF in these magnitude ranges by the fraction of good identifications.

7. COMPARISON TO BW AND GC LFs

We compare first the normalized K-band LF of the PGC with that of BW (Fig. 9). For $K_0 < 6.5$, we use the information from both Reg1 and Reg2 to improve the statistics. The LF for $K_0 > 6.5$ is constructed from Reg1 only. We use the

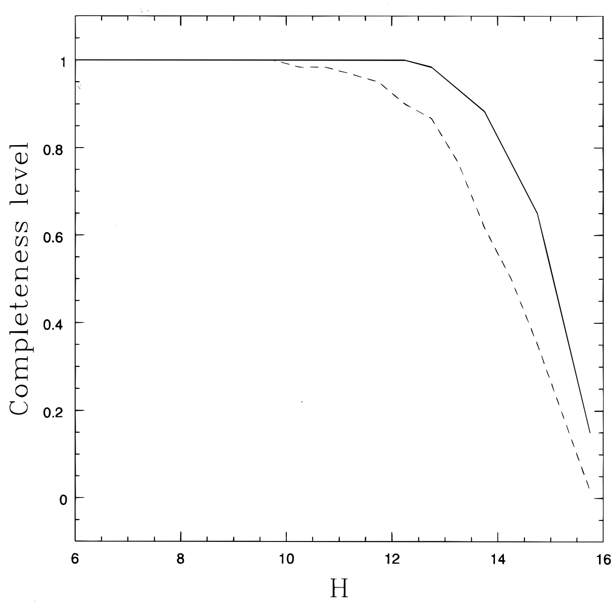

FIG. 7.—Completeness level as a function of H for the total star list (*solid line*) and the DAOPHOT star list (*dashed line*).

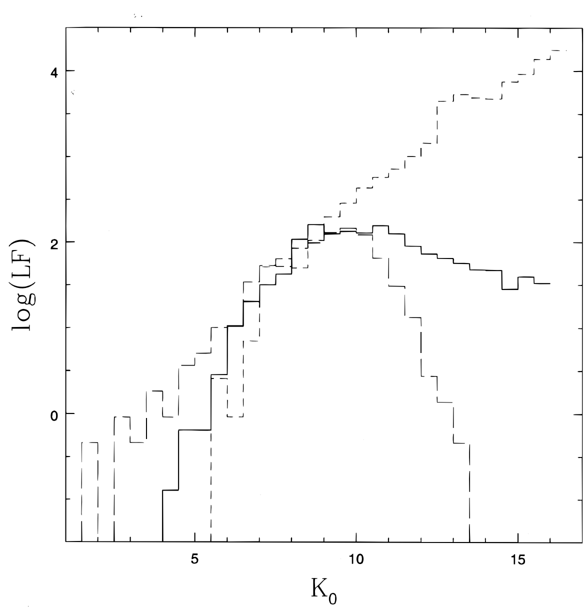

FIG. 9.—LFs of PGC (*solid line*), GC (*long-dashed line*), and BW (*short-dashed line*). For $K_0 < 6.5$, the PGC LF is constructed from both Reg1 and Reg2.

TABLE 4

EXPECTED NUMBER OF FOREGROUND M GIANTS TOWARD BW IN THE GRISM SURVEY OF FW87

	GJ MODEL		KENT MODEL		
MAGNITUDE	4 kpc	6 kpc	4 kpc	6 kpc	NUMBER OBSERVED
4.25	0.10	0.10	0.07	0.07	0
4.75	0.20	0.22	0.13	0.14	0
5.25	0.34	0.47	0.22	0.27	0
5.75	0.58	0.77	0.35	0.43	1
6.25	0.95	1.47	0.55	0.76	1
6.75	1.05	2.60	0.61	1.20	4
7.25	1.58	4.20	0.88	1.80	14
7.75	1.70	3.70	0.92	1.70	15
8.25	1.44	6.30	0.77	2.60	10
8.75	1.57	6.50	0.79	2.50	14

[a] For two different models of the star distribution, assuming distances to the bulge of 4 and 6 kpc: GJ (Garwood & Jones) and Kent (Kent et al. 1991).

BW LF from Tiede, Frogel, & Terndrup (1995), which is complete in the range $5.5 \leq K_0 \leq 16$. The bright end ($5.5 \leq K_0 \leq 9.0$) is derived by Frogel & Whitford (1987, hereafter FW87) from photometry of an unbiased subsample of the complete M giant surveys by Blanco, McCarthy, & Blanco (1984) and Blanco (1986). These surveys also included 10 long-period variables (LPVs). For $9.0 \leq K_0 < 12.5$, the BW LF is based on the data of DePoy et al. (1993b), who concluded that the M giants selected from the grism surveys by FW87 include essentially all stars with $K_0 \leq 10.0$ and that the FW87 field toward BW does not contain any other luminous stars. To compare the PGC and BW LFs, we normalize the latter to the total flux as follows: First we compute the total flux of the stars in the LF which have $M_{\rm bol} < -1.2$ (corresponding to $K_0 < 11.0$ at a distance to the GC of $R_0 = 8.0$ kpc). FW87 and Frogel (1988) conclude that this flux accounts for 60% of the total K-band light. Therefore, we divide this flux by 0.6 to obtain the total flux and use it to normalize the BW LF. Figure 9 also shows the GC LF obtained by Blum et al. (1996), who determined the relative normalization of the BW LF and GC LF.

Table 1 gives the three LFs together with the actual number of stars in each half-magnitude bin on which the LFs are based. Unlike the GC, the PGC LF does not extend brighter than $K_0 = 4.0$. In fact, we did not find a single star with a dereddened mag $K_0 < 4.0$ in either Reg1 or Reg2. In the entire field of the PGC, there was only one star in the range $3.5 < K_0 < 4.0$, and there were no stars brighter than $K_0 = 3.5$. In the range $4.0 \leq K_0 \leq 6.0$, the GC and PGC LFs are based on 43 and 33 stars, respectively. If the PGC LF were the same as the GC LF, we would expect $\sim 162 \pm 13$ stars in the range $4.0 \leq K_0 \leq 6.0$ inside Reg1 and Reg2, which is inconsistent with the actual number observed at the 9 σ level. The individual half-magnitude bins of the PGC LF are also deficient relative to the GC LF for all $K_0 < 6.0$.

The BW LF brighter than $K_0 = 7.0$ from Tiede et al. (1995) is based on a very small number of stars. Further, even these few bright stars with $K_0 < 7.0$ could be foreground stars (Tiede et al. 1995). We estimate the number of foreground stars expected in each half-magnitude bin for the grism survey of M giants used by FW87 for two different models of the disk LF. The FW87 field covers an area of 468 arcmin^2. The disk is assumed to have a radial scale length of 3 kpc in both the models (Kent, Dame, & Fazio 1991). The local density of different M giants given by Garwood & Jones (1987) is scaled appropriately to derive the density of these stars in any volume element along the line of sight to BW. In the first model (GJ model), the disk scale height of all the nine different spectral classes of M giants is taken to be 300 pc (Garwood & Jones 1987). In the second model, we assume a disk scale height of 165 pc for all the spectral classes (Kent et al. 1991). The expected foreground contamination in the FW87 field for observation cones extending to distances of 4 and 6 kpc is given in Table 4. This table also contains the number of M giants that are actually observed by FW87 in each half-magnitude interval. For $K_0 < 7.0$, the expected number of foreground M giants toward the BW in both models is comparable to the actual number of stars that are observed in the FW87 field. On the other hand, we find that the contamination of the PGC stars by foreground stars is negligible (<0.15 per half-magnitude bin). To understand this result, note that the total observed flux in the PGC regions corresponds to $K \sim 13.4$ mag arcsec^{-2}, corresponding to a dereddened surface brightness of $K \sim 10.7$ mag arcsec^{-2}. This is about 70 times brighter than BW with $K \sim 15.3$ mag arcsec^{-2}. Thus, although the absolute surface density of foreground disk stars is higher in the PGC than BW, the ratio of disk to

TABLE 5

PHOTOMETRY OF STARS IN PGC WITH $K_0 \leq 5$

Identification	$\Delta\alpha$ (arcsec)	$\Delta\delta$ (arcsec)	K	$H-K$	K_0	$(H-K)_0$
1	−80.4	−489.3	9.58	4.53	3.92	0.75
2	133.4	−243.9	9.41	3.92	4.56	0.68
3	255.0	379.9	10.17	4.36	4.64	0.67
4	98.3	−284.7	10.93	4.79	4.74	0.66
5	286.3	−439.9	7.73	2.60	4.81	0.65
6	−228.8	−106.4	10.83	4.62	4.87	0.65
7	118.0	390.8	7.86	2.63	4.88	0.65
8	406.3	−127.2	7.75	2.55	4.89	0.65
9	134.9	−281.1	10.82	4.59	4.90	0.64
10	−226.9	57.8	8.12	2.79	4.90	0.64
11	−446.0	169.9	8.85	3.26	4.91	0.64
12	−507.5	−16.3	8.77	3.21	4.93	0.64
13	−284.5	113.6	8.61	3.09	4.94	0.64
14	137.5	209.2	8.00	2.67	4.95	0.64
15	−157.7	136.4	7.55	2.36	4.96	0.64
16	438.1	290.8	8.98	3.30	4.98	0.64

bulge stars is much smaller. Even if all the six stars brighter than $K_0 = 7.0$ detected in the BW grism surveys are taken to be bulge stars, the PGC LF still contains a significant excess over the BW LF when all the bins in the range $5.5 < K < 7.0$ are combined. The PGC LF is therefore different from both the LF of the inner 2′ of the GC and the BW LF. It lies intermediate between the LFs of the GC and the BW for all $K_0 < 7.0$.

8. DISCUSSION

The stellar population of the GC has an excess of bright stars compared to the older population of BW (Haller 1992). The central parsec of the Galaxy contains helium-rich, luminous, blue, emission-line stars and Wolf-Rayet stars with estimated zero-age main-sequence masses of up to $\sim 100\ M_\odot$ (Allen, Hyland, & Hillier 1990; Krabbe et al. 1991; Blum, Sellgren, & DePoy 1995b; Blum, DePoy, & Sellgren 1995a; Libonate et al. 1995; Krabbe et al. 1995). A plausible scenario is a burst of star formation in the GC ~ 10 Myr ago (Krabbe et al. 1995). Krabbe et al. (1995) also concluded that the intermediate-mass asymptotic giant branch stars were formed in another burst of star formation ~ 100 Myr ago.

In the PGC, we do not find stars that are as luminous as the brightest stars in the GC. Nevertheless, there is a significant excess of stars with $K_0 \leq 7$ over the older population of the BW. This could imply the existence of a population of stars that is significantly younger than the old bulge population. The best way to confirm this hypothesis would be to take spectra of the bright stars in the PGC. To this end, we present in Table 5 a list of all stars with $K_0 < 5$ in the PGC region.

9. CONCLUSION

We have constructed the K-band LF of the perigalactocentric region outside the inner 2′ of the GC by dereddening individually every star using its observed $H-K$ colors. This LF is complete for $K_0 < 8$. Unlike the GC LF, this does not have any bright-end ($K_0 < 4.0$) component. There is also a deficiency in the PGC LF compared to the GC LF for all $K_0 \leq 6$. However, the PGC LF has a significant excess over the BW LF for $K_0 \leq 7$. We conclude that the PGC LF is intermediate between the GC and the BW LFs.

We thank Bob Blum, Jay Frogel, Kris Sellgren, and David Weinberg for helpful comments and suggestions. We also thank R. Bertram for his help with the observations. Work by A. G. was supported in part by NSF grant AST 94-20746. OSIRIS was constructed with support from the NSF grants AST 90-16112 and AST 92-18449.

REFERENCES

Allen, D. A., Hyland, A. R., & Hillier, D. J. 1990, MNRAS, 244, 706
Blanco, V. M. 1986, AJ, 91, 290
Blanco, V. M., McCarthy, M. F., & Blanco, B. M. 1984, AJ, 89, 636
Blum, R. D., DePoy, D. L., & Sellgren, K. 1995a, ApJ, 441, 603
Blum, R. D., Sellgren, K., & DePoy, D. L. 1995b, ApJ, 440, L17
———. 1996, ApJ, 470, 864
DePoy, D. L., Atwood, B., Byard, P., Frogel, J. A., & O'Brien, T. 1993a, Proc. SPIE, 1946, 667
DePoy, D. L., Terndrup, D. M., Frogel, J. A., Atwood, B., & Blum, R. 1993b, AJ, 105, 2121
Frogel, J. A. 1988, ARA&A, 26, 51
Frogel, J. A., & Whitford, A. E. 1987, ApJ, 320, 199 (FW87)
Garwood, R., & Jones, T. J. 1987, PASP, 99, 453
Haller, J. 1992, Ph.D thesis, Univ. Arizona
Kent, S. M., Dame, T. M., & Fazio, G. 1991, ApJ, 378, 131
Krabbe, A., Genzel, R., Drapatz, S., & Rotaciuc, V. 1991, ApJ, 382, L19
Krabbe, A., et al. 1995, ApJ, 447, L95
Libonate, S., Pipher, J. L., Forrest, W. J., & Ashby, M. L. N. 1995, ApJ, 439, 202
Mathis, J. S. 1990, ARA&A, 28, 37
Stetson, P. B. 1987, PASP, 99, 191
Tiede, G., Frogel, J. A., & Terndrup, D. M. 1995, AJ, 110, 2788